Progress In Electromagnetics Research M, Vol. 108, 139–149, 2022

A Miniaturized Dual-Band Circularly Polarized Implantable Antenna by Half-Cutting

Bo Yin[1, 2], Ming Ye[1, *], Junhao Cong[1], and Yingzhuo Xu[1]

Abstract—In this paper, a miniaturized dual-band circularly polarized (CP) implantable antenna is proposed. The −10 dB impedance bandwidth of the antenna in Industrial Scientific Medical (ISM) band and the low frequency part of UWB can reach 30.3% (2.02 ∼ 2.74 GHz) and 39.9% (3.73 ∼ 5.59 GHz), respectively. The important features are its CP characteristic in two bands and a small volume. The miniaturization of the antenna is realized by half-cutting technique, which is to cut the original antenna meeting the symmetry of structure and electric field distribution into two halves to obtain a compact structure and wider impedance bandwidth, so that the final size is $5 \times 10.4 \times 0.254\,\text{mm}^3$. The CP wave performance of the antenna is achieved by exciting orthogonal polarization components on the radiation surface. The proposed antenna provides an axial ratio of less than 3 dB. CP axial ratio bandwidths in the two bands are 24.4% and 18.1%, respectively. In addition, the safety considerations and link margin are evaluated to analyze the performance of the proposed antenna. In order to verify the simulation results, the proposed antenna is fabricated. The measurements are carried out under the human muscle mimicking liquid circumstances. The measured data are in good agreement with the simulation results.

1. INTRODUCTION

With the rapid development of mobile communications, antennas used in wireless communications are being studied by more and more scholars [1–4]. At the same time, the research on implantable antennas is gradually increasing. Human body communication is a short distance wireless communication technology around or inside the human body. Unlike others, it contains the nearest object around the human body, which may also be a part of the human body [5–7]. In this communication process, an implantable antenna plays a significant role in transmitting data [8–10]. For implantable antennas, many scholars have carried out researches in different directions to solve different problems. For example, increasing the antenna gain and reducing the coupling between devices [11, 12]. Dual-band implantable antenna can provide switching between a variety of different operating modes. Circularly polarized antenna has obvious anti-multipath effect, so it is necessary to design a CP implantable antenna with excellent performance. Therefore, the dual-band and CP characteristics of implantable antennas are very important in related research.

Dual-band antenna can provide two operating bands for the implanted device, so that the system has dual-mode working characteristics. Dual-modes can switch between wake mode and sleep mode, which requires less energy [13–17]. In [13], a helical radiation structure with two symmetric arms is used to achieve multi-band. It operates in 402 MHz MICS band, 1.6 GHz and 2.4 GHz ISM band, respectively, and its maximum bandwidth is 219 MHz. This design achieves multi-band resonance, but the bandwidth is relatively narrow. Similarly, in [14, 15], dual-band features are also achieved through multiple radiation structures, but they all have the problems of narrow-band and large size. In [16], a

Received 30 December 2021, Accepted 7 February 2022, Scheduled 18 February 2022

* Corresponding author: Ming Ye (2057299173@qq.com).

[1] School of Optoelectronic Engineering, Chongqing University of Posts and Telecommunications, Chongqing 400065, China.

[2] Institute for Advanced Sciences, Chongqing University of Posts and Telecommunications, Chongqing 400065, China.

dual-band implantable antenna operating in ISM band is proposed. Dual-band characteristic is realized by loading hexagonal and T-shaped gaps on the radiated metal plate. A conformal dual-band antenna is proposed in [17]. The spiral arm conformal with the capsule reduces the overall size. The antenna works in ISM band and low frequency part of ultra-wideband (UWB), which can achieve sufficient bandwidth. However, the CP characteristic for implanted antenna was not considered in these designs.

On the other hand, to mitigate polarization mismatch and multipath fading in human body area communication, CP implantable antenna is more suitable for implanted devices than linearly polarized (LP) antenna [18]. CP antenna has many advantages, such as anti-multipath effect, low bit error rate, and strong anti-interference ability. These advantages are especially applicable to scenarios where the relative position of the implantable antenna and the external antenna of the human body changes. Spiral structure, opening slots, cutting angle, etc. are often used to realize circular polarization of antenna [19–21]. In [19], a conformal wideband CP antenna is proposed for a WCE system. The antenna is wrapped around the inner wall of an ingestible capsule, and the helical structure forms a circularly polarized wave, achieving CP characteristic. The antenna is also wideband and miniaturized. Reference [20] proposed a dual-band CP implantable antenna firstly, which realized CP characteristics in two operating bands by introducing multiple gaps in the sinuous patch. In [21], a dual-band capsule antenna combining a reactive impedance substrate (RIS) and flexible material is proposed. The combination of surface waves generated by RIS and antenna radiation presents CP waves. The matching effect and axial ratio bandwidth are improved, but the integration of the RIS surface with the antenna adds complexity to the design. Another common technique is to excite orthogonal linearly polarized components with an orthogonal electric field and then introduce a 90° phase difference to generate CP waves [22–24]. Common ones are the use of orthogonal branches [22] and open L-shaped gaps [23].

In this paper, a miniaturized dual-band CP implantable antenna is proposed for the implanted system. This antenna uses multiple sinuous curves to form different current paths and excite two operating bands. The antenna operates in ISM band and low frequency part of UWB, and has CP characteristics in the two bands. CP wave is realized by generating orthogonal linearly polarized components from sinuous curves. At the same time, due to the use of half-cutting technology, the proposed antenna size is halved, but the dual-band and wideband characteristics are still maintained.

2. ANTENNA DESIGN AND ANALYSIS

2.1. The Structure of Antenna

The antenna designed in this paper is shown in Fig. 1. Fig. 1(a) shows the antenna with a symmetric structure. The half-cutting antenna is shown in Fig. 1(b). The dielectric substrate is Rogers RT/duroid 5880 with a thickness of 0.254 mm. As shown in Fig. 1, the radiation structure of the proposed antenna consists of several orthogonal metal branches, and the sixth branch (P6) is extended based on P5. In

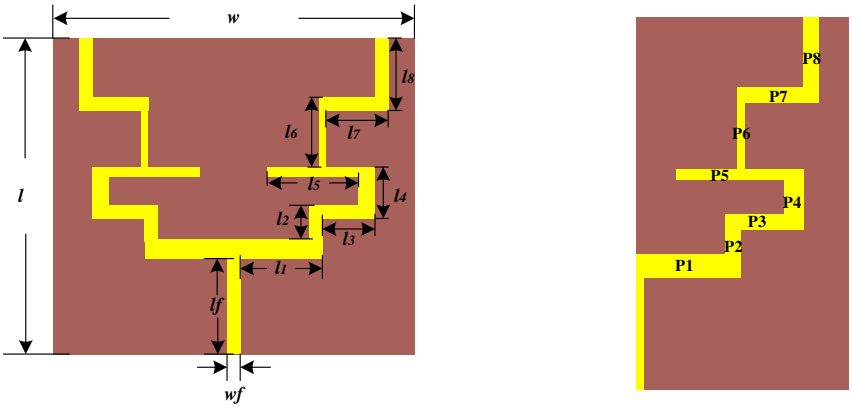

(a) (b)

Figure 1. (a) The antenna with symmetrical structure. (b) The half-cutting antenna.

this way, the current is split into two different paths as it passes through P5, resulting in two resonant frequencies. The first current path contains P1 $\rightarrow$ P5, and the second contains P1 $\rightarrow$ P8, which respectively excite the two resonant frequencies. The final antenna structure and parameters are shown in Fig. 1(b) and Table 1.

Table 1. Geometrical parameters of the proposed antenna. (units: mm).

Parameters	Values	Parameters	Values	Parameters	Values
l	10.4	l_3	2.4	l_7	2
w	10	w_3	0.3	w_7	0.3
l_f	3	l_4	1	l_8	2
w_f	0.4	w_4	0.5	w_8	0.5
l_1	2.5	l_5	3.6	h	0.254
w_1	0.3	w_5	0.3	d	1.8
l_2	1.2	l_6	2		
w_2	0.5	w_6	0.3		

Figure 2 shows the current distribution of the symmetrical antenna and half-cutting antenna at the same time. As can be seen from Fig. 2(a), the current distribution is symmetric along the axis. Meanwhile, the current distribution of the right part in Fig. 2(a) is basically consistent with that of the half-cutting antenna in Fig. 2(b). Some studies have shown that cutting the symmetrical monopole antenna in half can preserve its current path and broaden its bandwidth [25]. Based on this principle and symmetrical distribution of antenna current, the antenna is cut in half, and the half-cutting antenna in Fig. 1(b) is obtained. At this time, the half-cutting antenna can still maintain the resonant frequency uncharged. The S_{11} curves of two antennas are shown in Fig. 3. It can be seen that the half-cutting antenna matches better and have wider bandwidth.

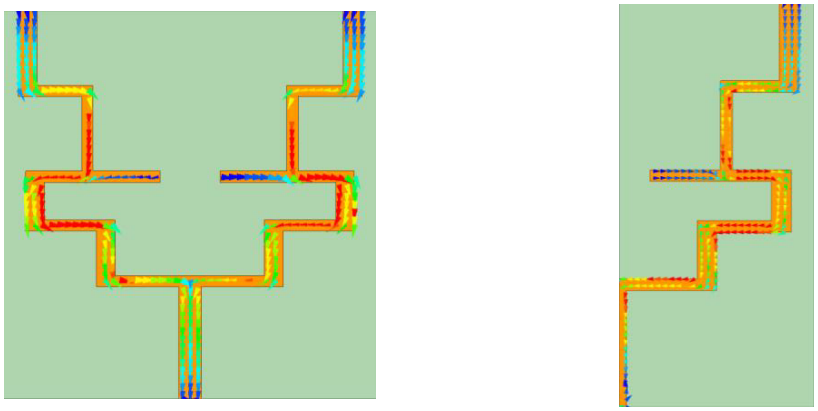

(a) (b)

Figure 2. Current distribution of antennas. (a) The antenna with symmetrical structure. (b) The half-cutting antenna.

It is notable that human tissue, where the antenna is implanted, is a lossy medium. According to the research data of Gabriel et al. [26], the electromagnetic characteristic parameters of human tissues are different from that of vacuum. Considering the actual working environment of the antenna, the simulation environment shown in Fig. 4 is set in High Frequency Structure Simulator (HFSS). The two antennas are respectively placed in two models for simulation.

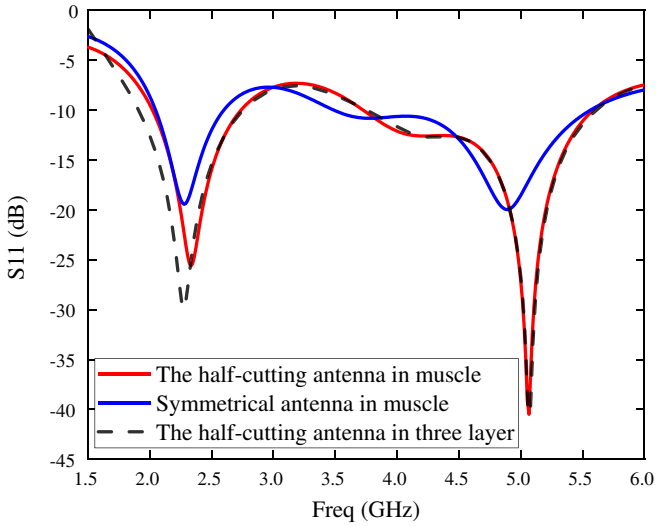

Figure 3. The S_{11} curves of two antennas.

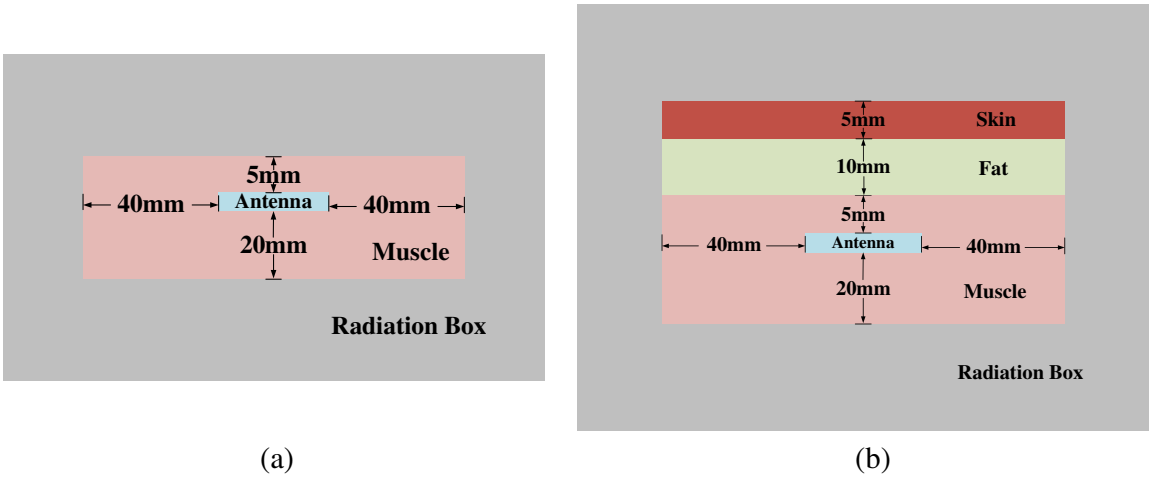

(a) (b)

Figure 4. Antenna simulation environment in HFSS. (a) Antenna in Muscle model. (b) Antenna in three layer model.

To analyze the sensitivity of proposed antenna, it is implanted in a muscle model and a three layer model. It can be seen from Fig. 3 that the proposed antenna can maintain good performance in both muscle model and three layer model, although there is a little frequency drift in three layer model. Table 2 shows the main performance of the antenna in the two models. It can be seen that the gain is lower in three layer model.

Table 2. Antenna performance implanted in two models. ($f_l = 2.45\,\text{GHz}$, $f_h = 5\,\text{GHz}$).

Model	Bandwidth (%)		Gain (dBi)	
	f_l	f_h	f_l	f_h
Muscle	30.3	39.9	−14.7	−17
Three layer	36.1	39.7	−22.3	−24

2.2. Circular Polarization Analysis

There are many ways for patch antenna to realize CP wave. The CP implantable antenna proposed in this paper is achieved by orthogonal electric field. As mentioned above, two current paths of the antenna excite two resonant frequencies, and each current path is composed of orthogonal branches. The introduction of multiple branches can not only increase the current path to reduce the size, but also realize the characteristics of CP waves. The dual CP performance of antenna is studied through the current distributions in different phases, as shown in Figs. 5 and 6. At 2.45 GHz, most of the current flows in the same path in the first patch (P1 $\rightarrow$ P8). At 5 GHz, however, the current flows in the second patch (P1 $\rightarrow$ P5). The figures show the current distributions at four time points in a period. The instantaneous current rotates counterclockwise, resulting in the performance of right hand circular polarization.

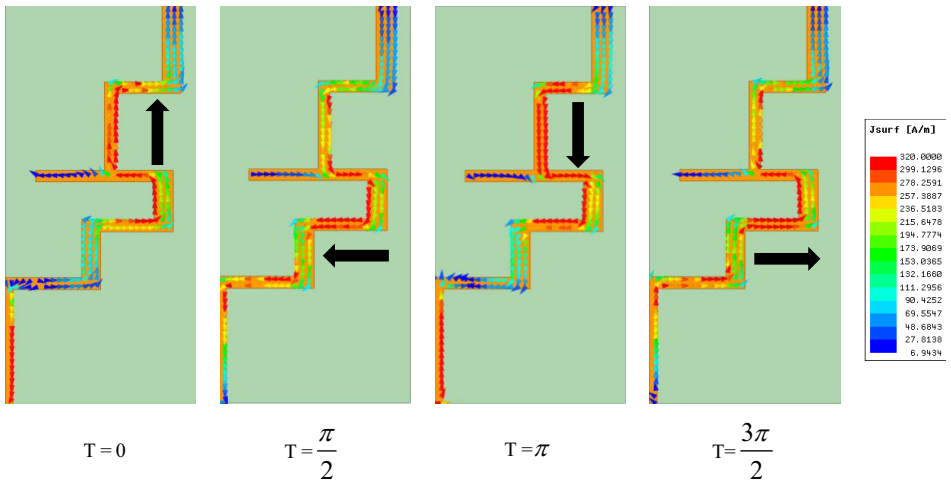

Figure 5. Current distributions of antenna at 2.45 GHz.

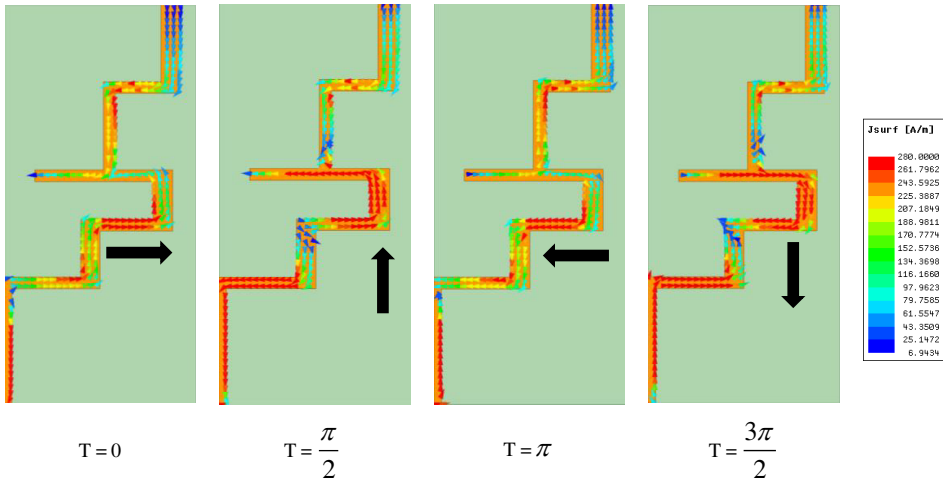

Figure 6. Current distributions of antenna at 5 GHz.

As can be seen from the figures, the antenna operates in the orthogonal mode. Multiple branches produce 90° phase differences and form a circularly polarized wave. Fig. 7 shows the radiation pattern of the antenna on the *xoz* plane. It can be seen that the main polarization of the antenna is right hand circular polarization. At 2.45 GHz, the maximum gain of right hand circular polarization is -14 dBi, and the cross-polarization ratio in the main radiation direction is 16 dB, which has good circular polarization

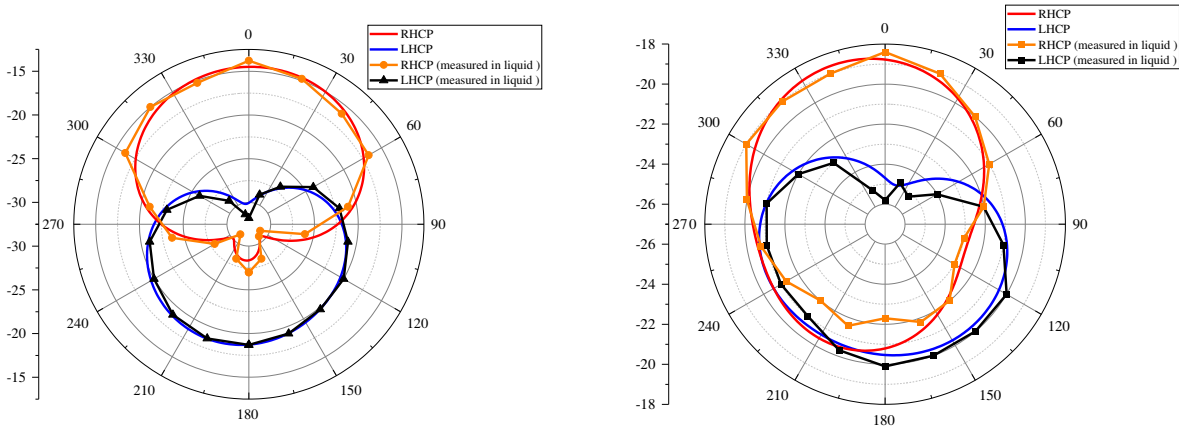

(a) 2.45 GHz (*xoz* plane) (b) 5 GHz (*xoz* plane)

Figure 7. The radiation pattern of proposed antenna at 2.45 GHz and 5 GHz.

purity. Similarly at 5 GHz, the maximum gain of right hand circular polarization is −18 dBi, and the cross-polarization ratio in the main radiation direction is 6 dB, which also has good circular polarization purity.

The CP performance of antenna is usually expressed as an axial ratio (AR) of less than 3 dB. The AR of proposed antenna is shown in Fig. 8. As shown in the figure, the 3 dB AR bandwidth covers ISM band and low frequency part of UWB and has a wide distribution range.

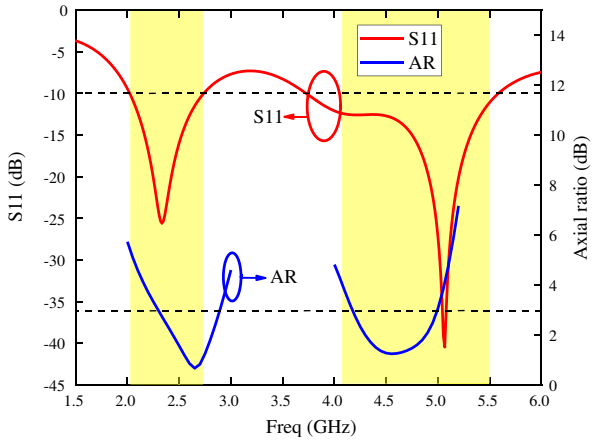

Figure 8. The AR of antenna.

2.3. SAR Distribution and Wireless Communication Link Margin

To investigate the safety of the proposed antenna in humans, the specific absorption rate (SAR) distribution of the proposed antenna is illustrated in Table 3. Assuming an input power of 1 W, the maximum average SARs (1 g tissue) are 628 and 643 W/kg in the muscle model, and 632 and 645 W/kg in three layer model at 2.45 GHz and 5 GHz, respectively. To reach the IEEE-specified human safety level limit of 1.6 W/kg, the maximum allowable input powers for muscle model and three layer model are 2.52 mW and 2.48 mW. Since the output power of commercial transmitters is much lower than the maximum allowable input power, SAR values in practical applications generally meet the IEEE safety limit [22].

Table 3. The maximum average SAR and maximum input power. ($f_l = 2.45\,\text{GHz}$, $f_h = 5\,\text{GHz}$).

Model	SAR (W/kg)		maximum input
	f_l	f_l	power (mW)
Muscle	628	643	2.52
Three layer	632	645	2.48

To evaluate the communication ability of the proposed antenna, the link margin is analyzed. The antenna performance in the three layer model is used for analysis, because the three layer model is more consistent with the actual application than the muscle model. According to Friis Transmission Formula, the link margin for far-field wireless communication is calculated as follows [27]:

$$\text{Link Margin (dB)} = Link\frac{C}{N_0} - Requied\frac{C}{N_0} \tag{1}$$

$$= (P_t + G_t - L_f + G_r - N_0) - \left(\frac{E_b}{N_0} + 10\log_{10} B_r - G_c + G_d\right) \tag{2}$$

$$L_f(\text{dB}) = 20\log_{10}\left(\frac{4\pi d}{\lambda}\right) \tag{3}$$

$$N_0 = 10\log_{10} k + 10\log_{10} T \tag{4}$$

where P_t is transmitting power, G_t the transmitting antenna gain, L_f the path loss, d the distance between the transmitting and receiving antennas, G_r the receiving antenna gain, N_0 the noise power density, and B_r the bit rate. Table 4 lists the parameters used to calculate the link margin.

Table 4. Communication link margin-related parameters.

Frequency (GHz)	2.45	5
Tx power (dBm)	-10	
Tx antenna gain G_t (dBi)	-22.3	-24
Rx antenna gain G_r (dBi)	2.15	
Boltzmann constant k	1.38×10^{-23}	
Ambient temperature T (K)	293	
Noise power density N_0 (dB/Hz)	-199.95	
E_b/N_0 (ideal PSK) (dB)	9.6	
Coding gain G_c (dB)	0	
Fixing deterioration G_d (dB)	2.5	

In this study, a 20 dB link margin is considered for reliable communication. The analysis of link margin at 2.45 GHz and 5 GHz is shown in Figs. 9(a) and (b).

It is can be seen in Fig. 9 (a) that at 2.45 GHz, the antenna can communicate at maximum distance of 14.5, 10.2, 7 m with bit rates of 10 kbps, 50 kbps, and 100 kbps, respectively. At 5 GHz, the maximum distance is 5.8, 4.3, 3 m, respectively.

3. FABRICATION AND MEASUREMENT

In order to verify the effectiveness of the antenna, symmetrical antenna and half-cutting antenna are fabricated and measured. The measuring device of antennas is shown in Fig. 10. The symmetrical antenna and half-cutting antenna are shown in Fig. 10(a), it is obvious that the size of the half-cutting

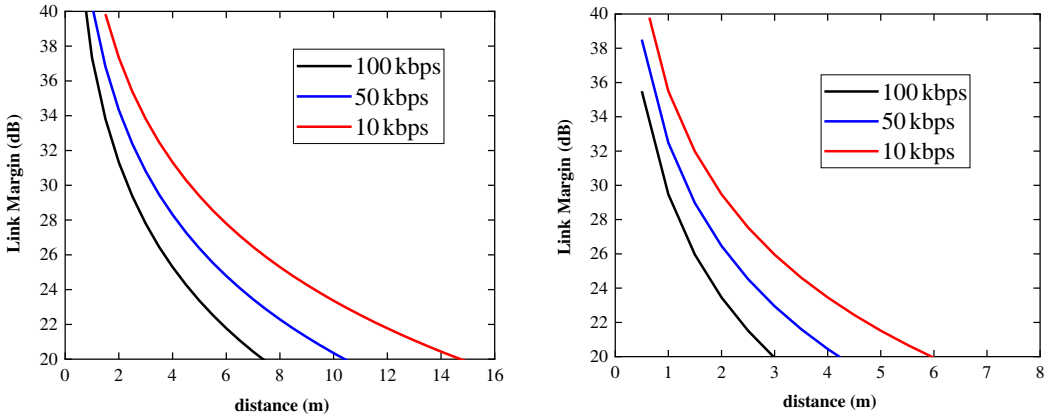

(a) 2.45 GHz (b) 5 GHz

Figure 9. Link margin with different bit rates.

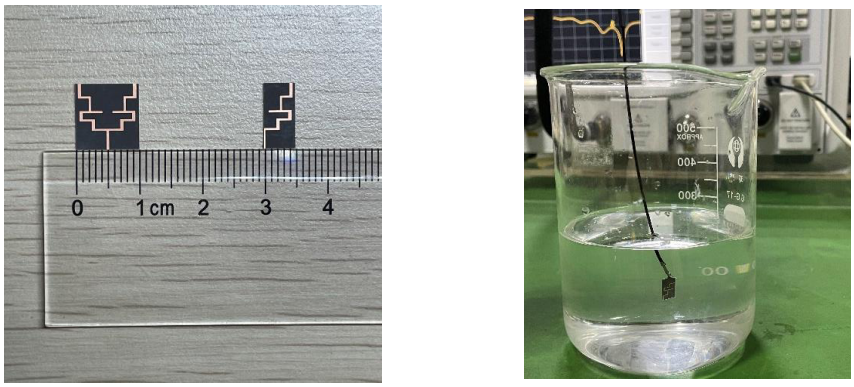

(a) (b)

Figure 10. Fabricated antennas and measurement setup. (a) The symmetrical UWB antenna and half-cutting antenna. (b) Measured in tissue mimicking liquid.

antenna is reduced. The antennas are measured in tissue mimicking liquid, as shown in Fig. 10(b), which are selected to replace the human tissue. The tissue mimicking liquid is prepared with propylene glycol, ethanol, sodium chloride, and deionized water, which is same as the electromagnetic properties of human muscle tissue.

As shown in Fig. 10(b), due to the small size of the antenna compared to the connector port, the feed port is extended with a 10 cm RF adapter (this connection is only used in the measuring process). The antennas are immersed into a tissue mimicking liquid at 5 cm deep for measurement. Agilent N5242A network analyzer is used as the measuring instrument. The operating frequency range of the instrument is 10 MHz $\sim$ 26.5 GHz.

Figure 11 illustrates the comparison of the measured and simulated results of the half-cutting antenna. It can be seen that the matching effect deteriorates in the tissue mimicking fluid, and the resonant frequency has some minor shifts. This error may be caused by the influence of SMA welding process.

The far field measurement of the antenna is in an anechoic chamber of the SATIMO16 probe. Similarly, tissue mimicking liquid is used to replace human muscle tissue, as shown in Fig. 12.

The AR of half-cutting antenna is measured. The measured results are shown in Fig. 13. It can be seen from the comparison that there is a little error between the measured and simulated values, which may be caused by the difference between the tissue mimicking liquid and the simulation environment.

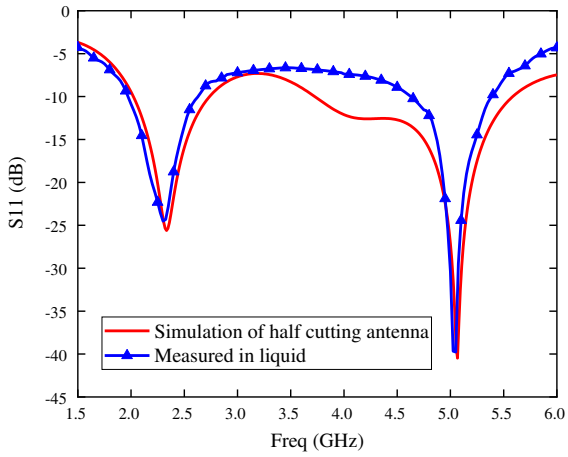

Figure 11. Comparison of simulation and measurement in liquid.

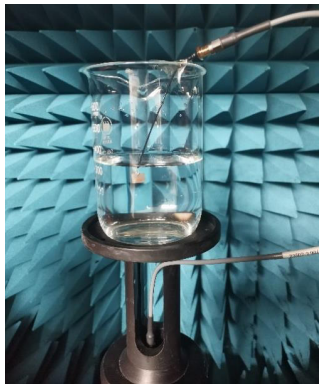

Figure 12. Far field measurement of antenna.

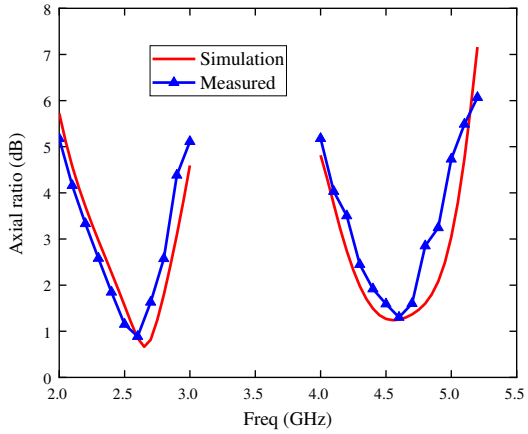

Figure 13. Comparison of simulation and measurement in liquid.

Table 5. Proposed antenna comparison with previous work.

Ref.	Freq (MHz)	I-BW (%)	AR-BW (%)	Gain (dBi)	SAR (W/kg)	Volume (mm^3)
18	2450	8.3	2.49	−22.7	–	120.7
19	915	20	29.2	−28.7	–	66.7
20	915 2450	13.63 6.28	33.0 8.67	−28.2 −24.5	420.3 233.2	2.11
21	920 2450	123	15.0 8.69	−29.3 −21.0	663 621	60.00
22	1400 2400	16.2	– 34.8	– –	– –	9.42
23	2400	8	19.1	−22.7	508	99.70
24	2450	16	18.3	−20.3	–	91.9
This paper	2450 5000	36.1 39.7	24.4 18.1	−22.3 −24.0	632 645	13.21

4. CONCLUSION

A compact, circularly polarized, dual-band implantable antenna is proposed. The size of the antenna is only $5 \times 10.4 \times 0.254\,\text{mm}^3$. Two operating frequency bands are realized by introducing two current paths. The circular polarization of the antenna is achieved by exciting the orthogonal linear polarization components of the sinuous branches. The simulation results show that the antenna has wide bandwidth and good circular polarization performance in ISM band and low frequency part of UWB. Through the calculation of link margin, the maximum communication distance of the antenna is analyzed. Compared with previously reported implantable antennas, the proposed antenna has a smaller volume, wider impedance bandwidth (I-BM) and axial ratio bandwidth (AR-BW), as shown in Table 5. Antennas are fabricated and placed in tissue mimicking liquid for measurement. The measured results show that the impedance bandwidth and axial ratio agree well with the simulated ones.

ACKNOWLEDGMENT

This work was supported by the Chongqing Graduate Research and Innovation Project (CYS20265).

REFERENCES

1. Saraswat, R. K. and M. Kumar, "A vertex-fed hexa-band frequency reconfigurable antenna for wireless applications," *International Journal of RF and Microwave Computer-Aided Engineering*, Vol. 29, e21893, 2019.
2. Saraswat, R. K. and M. Kumar, "Implementation of metamaterial loading to miniaturized UWB dipole antenna for WLAN and WiMAX applications with tunability characteristics," *IETE Journal of Research*, Vol. 2, 1–14, 2019.
3. Saraswat, R. K. and M. Kumar, "A metamaterial hepta-band antenna for wireless applications with specific absorption rate reduction," *International Journal of RF and Microwave Computer-Aided Engineering*, Vol. 29, e21824, 2019.
4. Saraswat, R. K. and M. Kumar, "Implementation of hybrid fractal metamaterial inspired frequency band reconfigurable multiband antenna for wireless applications," *International Journal of RF and Microwave Computer-Aided Engineering*, Vol. 30, e22315, 2020.
5. Greatbatch, W. and C. F. Holmes, "History of implantable devices," *IEEE Eng. Med. Biol.*, Vol. 10, No. 3, 38–41, 1991.
6. Islam, M. N. and M. R. Yuce, "Review of medical implant communication system (MICS) band and network," *ICT Express*, Vol. 2, No. 4, 188–194, 2016.
7. Zada, M., I. A. Shah, A. Basir, et al., "Ultra-compact implantable antenna with enhanced performance for leadless cardiac pacemaker system," *IEEE Trans. Antennas Propag.*, Vol. 69, No. 2, 1152–1157, 2021.
8. Asif, S. M., J. Hansen, M. S. Khan, S. D. Walden, et al., "Design and in vivo test of a batteryless and fully wireless implantable asynchronous pacing system," *IEEE Transactions on Biomedical Engineering*, Vol. 63, No. 5, 1070–1081, 2016.
9. Ahsan, N. K., C. Young-Ok, G. Henry, and H. Yang, "Recent advances in organ specific wireless bioelectronic devices: Perspective on biotelemetry and power transfer using antenna systems," *Engineering*, In Press, 2022.
10. Malik, N. A., P. Sant, T. Ajmal, and M. Ur-Rehman, "Implantable antennas for bio-medical applications," *IEEE Journal of Electromagnetics, RF and Microwaves in Medicine and Biology*, Vol. 5, No. 1, 84–96, 2021.
11. Singh, M. S., J. Ghosh, S. Ghosh, and A. Sarkhel, "Miniaturized dual-antenna system for implantable biotelemetry application," *IEEE Antennas and Wireless Propagation Letters*, Vol. 20, No. 8, 1394–1398, 2021.

12. Ghosh, J. and D. Mitra, "Restoration of antenna performance in the vicinity of metallic cylinder in implantable scenario," *IET Microwaves Antennas & Propagation*, Vol. 14, No. 12, 1440–1445, 2020.
13. Shah, I. A., M. Zada, and H. Yoo, "Design and analysis of a compact-sized multiband spiral-shaped implantable antenna for scalp implantable and leadless pacemaker systems," *IEEE Trans. Antennas Propag.*, Vol. 67, No. 6, 4230–4234, 2019.
14. Soontornpipit, P. and P. Satitvipawee, "Design and development of a dual-band PIFA antenna for wireless biotelemetry applications," *2018 International Electrical Engineering Congress, iEECON*, 1–4, 2018.
15. Bao, Z., Y. X. Guo, and R. Mittra, "Single-layer dual-/tri-band inverted-f antennas for conformal capsule type of applications," *IEEE Trans. Antennas Propag.*, Vol. 65, No. 12, 7257–7265, 2017.
16. Faisal, F., M. Zada, A. Ejaz, et al., "A miniaturized dual-band implantable antenna system for medical applications," *IEEE Trans. Antennas Propag.*, Vol. 68, No. 2, 1161–1165, 2020.
17. Liu, K., R. P. Liu, W. J. Cui, et al., "Design of conformal spiral dual-band antenna for wireless capsule system," *IEEE Access*, Vol. 9, 117349–117357, 2021.
18. Li, R., Y. X. Guo, B. Zhang, and G. Du, "A miniaturized circularly polarized implantable annular-ring antenna," *IEEE Antennas and Wireless Propagation Letters*, Vol. 16, 2566–2569, 2017.
19. Das, R. and H. Yoo, "A wideband circularly polarized conformal endoscopic antenna system for high-speed data transfer," *IEEE Trans. Antennas Propag.*, Vol. 65, No. 6, 2816–2826, 2017.
20. Hayat, S., S. A. A. Shah, and H. Yoo, "Miniaturized dual-band circularly polarized implantable antenna for capsule endoscopic system," *IEEE Trans. Antennas Propag.*, Vol. 69, No. 4, 1885–1895, 2021.
21. Samanta, G. and D. Mitra, "Dual-band circular polarized flexible implantable antenna using reactive impedance substrate," *IEEE Trans. Antennas Propag.*, Vol. 67, No. 6, 4218–4223, 2019.
22. Duan, Z. and L. J. Xu, "Dual-band implantable antenna with circular polarisation property for ingestible capsule application," *Electronics Letters*, Vol. 53, No. 16, 1090–1092, 2017.
23. Xu, L. J., Y. Bo, W. J. Lu, et al., "Circularly polarized annular ring antenna with wide axial-ratio bandwidth for biomedical applications," *IEEE Access*, Vol. 7, 59999–60009, 2019.
24. Xu, L. J., J. P. Xu, Z. J. Chu, et al., "Circularly polarized implantable antenna with improved impedance matching," *IEEE Antennas and Wireless Propagation Letters*, Vol. 19, No. 5, 876–880, 2020.
25. Mobashsher, A. T. and A. Abbosh, "Utilizing symmetry of planar ultra-wideband antennas for size reduction and enhanced performance," *IEEE Antennas and Propagation Magazine*, Vol. 57, No. 2, 153–166, 2015.
26. Gabriel, S., R. W. Lau, and C. Gabriel, "The dielectric properties of biological tissues: III. Parametric models for the dielectric spectrum of tissues," *Physics in Medicine and Biology*, Vol. 41, No. 11, 2271–2293, 1996.
27. Xia, W., K. Saito, M. Takahashi, and K. Ito, "Performances of an implanted cavity slot antenna embedded in the human arm," *IEEE Trans. Antennas Propag.*, Vol. 57, No. 4, 894–899, 2009.